
PAI-Conv: Permutable Anisotropic Convolutional Networks for Learning on Point Clouds

Zhongpai Gao, Guangtao Zhai, Junchi Yan, Xiaokang Yang

Artificial Intelligence Institute, Shanghai, China

Shanghai Jiao Tong University

Shanghai, 200240, China

{gaozhongpai, zhaiguangtao, yanjunchi, xkyang}@sjtu.edu.cn

Abstract

Demand for efficient representation learning on point clouds is increasing in many 3D computer vision applications. The recent success of convolutional neural networks (CNNs) for image analysis suggests the value of adapting insight from CNN to point clouds. However, unlike images that are Euclidean structured, point clouds are irregular since each point's neighbors vary from one to another. Various point neural networks have been developed using isotropic filters or applying weighting matrices to overcome the structure inconsistency on point clouds. However, isotropic filters or weighting matrices limit the representation power. In this paper, we propose a permutable anisotropic convolutional operation (PAI-Conv) that calculates soft-permutation matrices for each point according to a set of evenly distributed kernel points on a sphere's surface and performs shared anisotropic filters as CNN does. PAI-Conv is physically meaningful and can efficiently cooperate with random point sampling method. Comprehensive experiments demonstrate that PAI-Conv produces competitive results in classification and semantic segmentation tasks compared to state-of-the-art methods.

1 Introduction

Point clouds are the simplest shape representation for 3D geometric data and are the raw output of many 3D acquisition devices, e.g., LiDAR scanners. Feature learning from point clouds is crucial for many applications, such as 3D object detection [8, 33, 58], 3D object classification and segmentation [34, 26, 50, 43], 3D shape generation and correspondence [13, 10], and motion estimation of driving scenes [49]. Inspired by the great success of convolutional neural networks (CNN) in the fields of natural language processing (1-D), image classification (2-D), and radiographic image analysis (3-D) where underlying data are Euclidean structured, deep neural networks on point clouds have recently driven significant interests. Directly applying CNN on point clouds is a challenge since they are non-Euclidean structured and the number and orientation of each point's neighbors vary from one to another. An effective definition of convolutional operation analogous to that on Euclidean structured data is important for feature learning on point clouds.

Recently, many deep neural networks have been developed to handle point clouds and achieved promising results. PointNet [34] designed a deep learning framework that operates on each point individually and aggregates all individual point features to a global signature. However, the local structure of point clouds is not exploited. DGCNN [50] proposed a neural network module that explicitly constructs a local graph and learns embeddings for the edges to capture local geometric structure. However, DGCNN [50] applies isotropic filters over each point's neighbors, which limits the representation power compared to CNN.

Several works have introduced anisotropic filters for point cloud processing. PointCNN [26] proposed to learn an \mathcal{X} -transformation from the input points to weight and permute each point's neighbors

into a latent and potentially canonical order. KPConv [43] presented a convolutional operation that weights each point’s neighbors depending on the Euclidean distances to a set of predefined or deformable kernel points. Subsequently, these methods apply anisotropic filters on the resampled neighbors to extract features for point clouds. However, these methods do not explicitly explain why the transformation learned from the input points or the weighting matrix calculated from the kernel points can rearrange the irregular point clouds into regular and structured data so that anisotropic filters are able to take effect.

In this paper, we propose a **permutable anisotropic convolutional operator (PAI-Conv)** for point clouds. We generate a set of kernel points that are evenly distributed on the surface of a sphere using Fibonacci lattice [12] as a reference of the canonical order. For each point, we calculate the dot product between each point’s neighbors and the kernel points and then apply Sparsemax activation function [29] to obtain a sparse soft-permutation matrix. No weight is to learn for the sparse-soft permutation matrix. Mathematically, applying dot product and Sparsemax activation function resamples and reorders the local neighbors according to the orientations of the kernel points so that the convolutional neighbors follow the canonical order determined by orientation order of the kernel points. Then similar to CNN, we apply shared anisotropic filters on the convolutional neighbors to extract local features on point clouds. PAI-Conv is designed to explicitly resample and reorder the neighbors and is physically meaningful.

Thanks to its design, PAI-Conv works efficiently with random point sampling method instead of using other complex sampling approaches, which is efficient and can be applied in large-scale point clouds. We use PAI-Conv as a basic building module in existing frameworks and achieve state-of-the-art performance in classification and segmentation on several datasets. The main contributions of this paper are summarized below:

- We propose a novel convolution operation for representation learning from point clouds, **permutable anisotropic convolution (PAI-Conv)**, to better capture local geometric features of 3D shapes.
- PAI-Conv works efficiently with random point sampling method and can be implemented and integrated into existing pipelines for point cloud processing.
- Extensive experiments show that our model achieves state-of-the-art performance for classification and segmentation on point clouds.

2 Related work

Graph neural networks Closely related to point clouds, graph data are also irregular but with edge connections. Graph neural networks are approaches to generalize CNN to irregular graph-structured data. Spatial-based approaches define graph convolutions based on a node’s spatial relations. DCNN [2] assumes information is transferred from one node to its neighbors with a certain transition probability and regards graph convolutions as a diffusion process. GraphSage [15] adopts sampling to obtain a fixed number of neighbors for each node. GAT [45] adopts attention mechanisms to learn the relative weights between two connected nodes. MoNet [32] introduces node pseudo-coordinates to determine the relative position between a node and its neighbors and assigns different weights to the node’s neighbors. FeaStNet [46] proposed a graph-convolution operator that learns a weighting matrix dynamically computed from features.

Transformer Transformer models [44] have demonstrated great success across a wide range of applications, especially for natural language processing (NLP) [11]. In Transformer models for NLP, a sentence (i.e., a sequence of words) is considered as a fully-connected graph and Transformer can be considered as one kind of graph neural networks. As shown in Fig. 1, the dot product self-attention is both used in PAI-Conv and Transformer. Compared to Transformer, PAI-Conv uses local neighboring position as the query, a set of fixed kernel points as the key, point features as the value, and Sparsemax as the activation function.

Point neural networks Deep learning on point clouds has drawn great attention recently. PointNet [34] proposed an efficient architecture that directly applies multi-layer perceptrons (MLP) on each point. However, PointNet does not capture local structures from point clouds. Many neighboring feature pooling methods [25, 56, 55] have been presented. PointNet++ [36] proposed to sample points in a hierarchical fashion. DGCNN [50] proposed a convolutional operation that generates edge

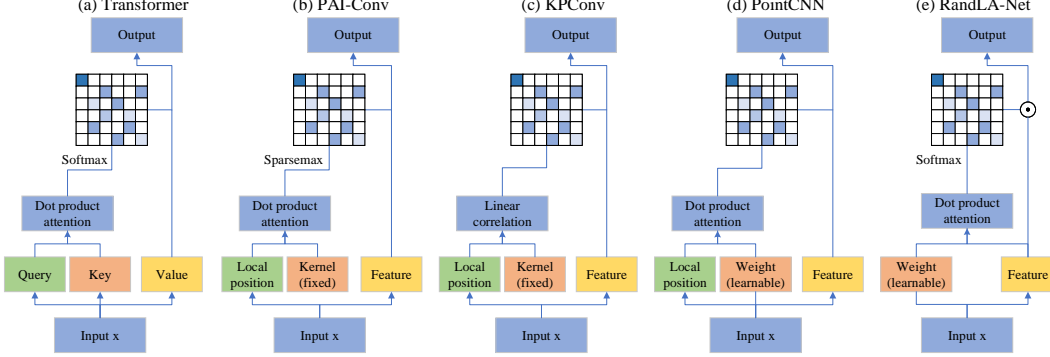


Figure 1: Architecture comparison to some existing methods.

features to describe the relationships between a point and its neighbors. PointCNN [26] presented a method to learn an \mathcal{X} -transformation as a function of input points. RandLA-Net [16] uses an attention mechanism to learn local features instead of applying filters for convolutional operation. Besides, many kernel-based convolutional methods [39, 17, 24, 21, 22, 28] have been proposed. KPConv [43] proposed a convolution that takes radius neighbors as input and processes them with weights spatially located by a set of kernel points.

For KPConv [43], instead of calculating a soft-permutation matrix from the kernel points using the dot product attention, KPConv calculates a weighting matrix using linear correlation with an extra hyperparameter σ . The hyperparameter σ is difficult to control since the input density may not be constant and a small variation of σ may significantly affect the weighting matrix. Furthermore, the dot product in PAI-Conv is more computationally efficient than the linear correlation in KPConv. At last, different from weighting matrices, PAI-Conv applies Sparsemax to obtain sparse soft-permutation matrices to explicitly permute each point’s neighbors into canonical order. For PointCNN [26], instead of using kernel points to determine the canonical order, PointCNN learns transformation matrices from each point’s neighbors using MLP. The weights of MLP can be considered as learnable kernel points, where the idea is similar to deformable KPConv [43]. However, it is difficult to stabilize the learnable kernel points when they are trained along with the whole network. Furthermore, the learnable matrix is not constrained by any forms to act as a transformation matrix to permute the point’s neighbors into canonical order.

3 Our approach

Inspired by the conventional convolution on Euclidean structured data, we propose a permutable anisotropic convolutional operation (PAI-Conv) on point clouds. Instead of directly applying anisotropic filters on each point’s neighbors, we rearrange each point’s neighbors using a soft permutation matrix that is calculated based on each point’s neighbors and a set of predefined kernel points. Then similar to CNN, we apply anisotropic filters to extract features from point clouds.

3.1 Permutable anisotropic convolution

Consider a point cloud $\mathcal{P} = \{p_1, \dots, p_N\}$ with per-point features $\mathbf{f} \in \mathbb{R}^D$, where D and N represents the feature dimension and number of points, respectively. Each point contains 3D coordinates $\mathbf{p}_i = [x_i, y_i, z_i]^\top$ in the Euclidean space. Point features can include RGB color or intermediate learned features in a deep neural network. For each point, its neighboring points are gathered by the simple K-nearest neighbors (KNN) algorithm based on the point-wise Euclidean distances for efficiency. We denote the i th point’s K -nearest neighbors as $\mathcal{N}_i = \{p_i, p_{i,1}, \dots, p_{i,K-1}\}$. PAI-Conv is as defined follows.

Soft-permutation matrix We generate a set of kernel points by mapping the Fibonacci lattice [12] onto the surface of a sphere via equal-area projection so that the kernel points are evenly distributed on a sphere, denoted as $\mathcal{K} = \{k_0, k_1, \dots, k_{L-1}\}$, where $k_0 = [0, 0, 0]^\top$ is at the origin and L is the number of kernel points. For the i th point, we obtain the local neighboring positions of the neighbors as $\tilde{\mathbf{p}}_{i,j} = \mathbf{p}_i - \mathbf{p}_{i,j}$, where $\mathbf{p}_{i,j} \in \mathcal{N}_i$ and $\tilde{\mathbf{p}}_{i,0} = [0, 0, 0]^\top$ is at the origin. As shown

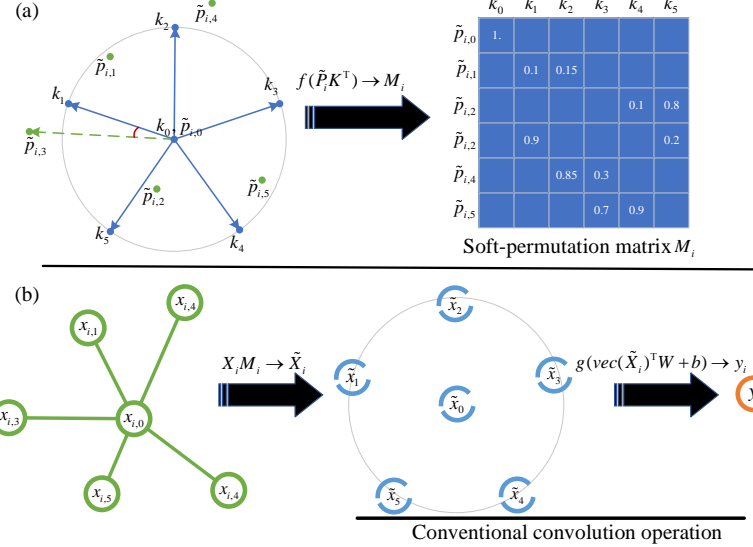


Figure 2: Permutable anisotropic convolutional operation (PAI-Conv). $\{k_0, k_1, \dots, k_{L-1}\}$ are the predefined kernel points. $\{\tilde{p}_{i,0}, \tilde{p}_{i,1}, \dots, \tilde{p}_{i,K-1}\}$ are the local neighboring positions of point p_i . The permutation matrix M_i is calculated by the dot product of the local neighboring positions and the kernel points followed by Sparsemax activation function $f(\cdot)$. $\{x_{i,0}, x_{i,1}, \dots, x_{i,5}\}$ are the point features of point p_i 's neighbors. PAI-Conv uses the soft-permutation matrix, $M_i \in \mathbb{R}^{K \times L}$, to resample the node's neighbors. Then, a conventional convolution operation with anisotropic filters followed by ELU activation function $g(\cdot)$ is performed. The anisotropic filters have weights $W \in \mathbb{R}^{(D_{in} \cdot L) \times D_{out}}$ and bias $b \in \mathbb{R}^{D_{out}}$.

in Figure 2a, the soft-permutation matrix is simply calculated by the dot product between the local neighboring positions and the kernel points followed by Sparsemax activation function [29], which can be expressed as

$$M_i = f(\tilde{P}_i K^T), \quad (1)$$

where $\tilde{P}_i \in \mathbb{R}^{K \times 3}$, $K \in \mathbb{R}^{L \times 3}$, $M_i \in \mathbb{R}^{K \times L}$, and $f(\cdot)$ is the Sparsemax activation function. For each kernel point, the dot product ensures a local neighboring position with a smaller angle to the kernel point has a larger weight. The Sparsemax activation function ensures the soft-permutation matrix is sparse and only those points with small angles to a kernel point are selected otherwise the weight is zero. For example, as shown in Figure 2a, $\tilde{p}_{i,3}$ and $\tilde{p}_{i,1}$ have small angles to k_1 and are assigned with weight of 0.9 and 0.1, respectively. Other points with larger relative angles are assigned with weight of zero. Note that, since $k_0 = \tilde{p}_{i,0} = [0, 0, 0]^T$, the dot product of these two vectors is zero. We need to set $M[0, 0] = 1$ to make the point itself be selected as the first point in the resample convolutional neighbors.

Point feature Inspired by RandLA-Net [16], we first encode the relative point position as

$$r_{i,j} = MLP(p_i \oplus (p_i - p_{i,j}) \oplus \|p_i - p_{i,j}\|), \quad (2)$$

where \oplus is the concatenation operation and $\|\cdot\|$ calculates the Euclidean distance between the neighbors and the center point. Then, the point feature is obtained by concatenating the relative point position and the per-point features as follows,

$$x_{i,j} = r_{i,j} \oplus f_{i,j}, \quad (3)$$

where $f_{i,j}$ is the RGB color or intermediate learned features as mentioned above, $x_{i,j} \in \mathbb{R}^{D_{in}}$, and D_{in} is the feature dimension. For each point, we construct $X_i = \{x_{i,0}, x_{i,1}, \dots, x_{i,K-1}\} \in \mathbb{R}^{D_{in} \times K}$ for the convolutional operation.

Since the order and orientation of each point's neighbors vary from one to another, directly applying an anisotropic filter on unordered neighbors diminishes the representation power. While training,

the anisotropic filter might struggle to adapt to the large variability of the unordered coordinate systems and the possibility of learning rotation invariant filter increases. In this paper, we resample each point’s neighbors using the soft-permutation matrix in Eq. (1). The resampled convolutional neighbors of each point can be obtained by

$$\tilde{\mathbf{X}}_i = \mathbf{X}_i \mathbf{M}_i, \quad (4)$$

where $\tilde{\mathbf{X}}_i \in \mathbb{R}^{D_{in} \times L}$. Since the point’s neighbors are rearranged according to the canonical order of predefined kernel points, we can apply a shared anisotropic filter on each point of a point cloud. This operation is the same as the conventional convolution and can be expressed as

$$\mathbf{y}_i = g(\text{vec}(\tilde{\mathbf{X}}_i)^\top \mathbf{W} + \mathbf{b}), \quad (5)$$

where $\mathbf{W} \in \mathbb{R}^{(D_{in} \cdot L) \times D_{out}}$ includes D_{out} anisotropic filters, $\mathbf{b} \in \mathbb{R}^{D_{out}}$ is the bias, $\mathbf{y}_i \in \mathbb{R}^{D_{out}}$ is the output feature point corresponding to the input feature point $\mathbf{x}_i \in \mathbb{R}^{D_{in}}$, $\text{vec}(\cdot)$ is a vectorization function which converts a matrix into a column vector, and $g(\cdot)$ is an activation function, e.g., ELU [9], to introduce non-linearity.

3.2 Properties

Intuitively, **anisotropic filter** and **permutation invariance** are two mutually exclusive properties. Using anisotropic filter requires each point’s neighbors are sorted in a certain way while permutation invariance means we can randomly change the order of each point’s neighbors. The proposed PAI-Conv resolves these two incompatible properties by introducing soft-permutation matrices so that the initial order of each point’s neighbors is not important. PAI-Conv achieves permutation invariance both for the order of points in a point cloud and the order of each point’s neighbors. KNN makes sure each point has the same neighbors even we reshuffle the order of points in a point cloud. The dot product attention and Sparsemax activation function make sure the calculated soft-permutation matrix can rearrange the neighbors in the canonical order defined by the kernel points even we reshuffle the order of each point’s neighbors. Since each point’s neighbors follow the same canonical order, we can apply anisotropic filters to extract local features with high representation power for point clouds.

4 Experiments

In this paper, we evaluate the models constructed using PAI-Conv for two different tasks: classification and semantic segmentation. Ablation tests are conducted to demonstrate the effectiveness of the architecture design.

4.1 Classification

We evaluate our model on the ModelNet40 [53] for the classification task. The dataset contains 12,311 meshed CAD models from 40 clauses: 9,843 models for training and 2,468 models for testing. The Mean Accuracy (MA) and Overall Accuracy (OA) of all classes are used as the standard metrics. We test PAI-Conv in two different data sampling methods: uniformly sampling and randomly sampling.

4.1.1 Uniformly sampling data

Data. Following the experimental setting of [34, 50], we uniformly sample 2,048 points on mesh faces according to the face area and normalize them into a unit sphere. The training data are augmented on-the-fly by randomly scaling points in the range of [2/3, 3/2], translating points in the range of [-0.2, 0.2], and jittering points by Gaussian noise with zero mean and 0.01 standard deviation.

Architecture. We adopt the network architecture from [50] and replace the EdgeConv with our proposed PAI-Conv, where the size of kernel points is $L = 32$ and each point’s neighbors is $K = 40$. First, soft-permeation matrices for each point are computed. We use four PAI-Conv layers with channels of [64, 64, 128, 256] to extract geometric features. Since no down-sampling is applied in the network, the four PAI-Conv layers share the same neighboring indexes and soft-permutation matrices. Shortcut connections are included to extract multi-scale features and one shared MLP layer [2048] is used to aggregate multi-scale features. Then, we use max/sum pooling along the dimension of point cloud’s size to get the global feature. At last, two fully-connected layers with channels of [512, 40] and two dropout layers with 0.5 probability are used to finally predict a 3D shape’s class.

Table 1: Classification results on ModelNet40. The metrics we used are mean accuracy (MA) and overall accuracy (OA).

| | MA | OA | | MA | OA |
|---------------------------|-------------|-------------|--------------------------|-------------|-------------|
| 3DShapeNets [53] | 77.3 | 84.7 | PointNet [34] | 86.0 | 89.2 |
| VoxNet [30] | 83.0 | 85.9 | PointNet++ [36] | - | 90.7 |
| Subvolume [35] | 86.0 | 89.2 | Kd-net [20] | - | 90.6 |
| VRN [6] | - | 91.3 | PointCNN [26] | 88.1 | 92.2 |
| ECC [38] | 83.2 | 87.4 | PCNN [3] | - | 92.3 |
| SpecGCN [47] | - | 91.5 | KPConv [43] | - | 92.9 |
| Uniformly Sampling | | | Randomly Sampling | | |
| DGCNN [50] | 90.7 | 93.5 | DGCNN [50] | 89.0 | 92.4 |
| RandLA-Net [16] | 84.7 | 89.8 | RandLA-Net [16] | 86.1 | 90.7 |
| PAI-Conv (Ours) | 90.0 | 93.2 | PAI-Conv (Ours) | 90.5 | 93.2 |

Training. We use SGD optimizer with an initial learning rate 0.1 and schedule the learning rate to be ended at 0.01 using cosine annealing method [27] for 250 epochs. The batch size is 16 and the momentum is 0.9.

Results. Table 1 shows the classification results on ModelNet40. Our proposed PAI-Conv is competitive against state-of-the-art methods. When the point clouds are uniformly sampled, PAI-Conv achieves the results that are only slightly lower than DGCNN [50]. Since the point clouds are uniformly sampled, the neighbors of each point are evenly distributed, making anisotropic filters in PAI-Conv redundant. Thus, the advantage of PAI-Conv over DGCNN is not well exploited. However, uniformly sampling data is computationally expensive, which is not practical for large scale point clouds in many applications.

4.1.2 Randomly sampling data

Instead of relying on expensive sampling techniques or computationally heavy pre/post- processing steps, we randomly sample 8192 points from each point cloud. The same network architecture and training procedure as in Section 4.1.1 are used. Through the four PAI-Conv layers, the point cloud is down-sampled randomly with the ratios of [4, 4, 2, 2]. Since the point cloud is down-sampled, the neighboring indexes and soft-permutation matrices are calculated for each PAI-Conv layer.

Table 1 also shows the classification results on ModelNet40 when the point clouds are randomly sampled. PAI-Conv achieves better results than DGCNN [50]. Randomly sampling data is efficient and can easily be applied to large-scale point clouds. The total time and memory consumption comparisons of different sampling methods are demonstrated in Figure 5 of [16]. We re-implement RandLA-Net [16] in both uniformly and randomly sampling methods. PAI-Conv outperforms RandLA-Net in a large margin in the classification task.

4.2 Semantic segmentation

In this section, we evaluate our model for the semantic segmentation task on three large-scale public datasets as follows:

SemanticKITTI dataset [4] The SemanticKITTI consists of 22 sequences of densely annotated LiDAR scans: sequence 00-07 and 09-10 with 19,130 scans for training, sequence 08 with 4,071 scans for validation, and sequence 11-21 with 20,351 scans for testing. Each scan is a large-scale point cloud with around 10^5 points and up to $160 \times 160 \times 20$ meters in 3D space. The SemanticKITTI dataset only includes 3D coordinates without other feature information. The Mean Intersection-over-Union (mIoU) score over 19 categories is used as the standard metric.

Semantic3D dataset [14] The Semantic3D consists of 30 terrestrial laser scans: 15 for training and 15 for testing. Each point cloud has up to 10^8 points and takes up to $160 \times 240 \times 30$ meters in 3D space. The Semantic3D dataset includes 3D coordinates and RGB information that are used as the input for training and testing. The mIoU and OA of all 8 classes are used as the standard metrics.

S3DIS dataset [1] The S3DIS consists of 6 large-scale indoor areas from three different buildings: 5 for training and 1 for testing using the standard 6-fold cross-validation. Each point cloud is a

Table 2: Quantitative results on SemanticKITTI [4].

| Size | Methods | mIoU(%) | | road | sidewalk | parking | other-ground | building | car | truck | bicycle | motorcycle | other-vehicle | vegetation | trunk | terrain | person | bicyclist | motorcyclist | fence | pole | traffic-sign |
|------------------------|-------------------|-------------|------|-------------|-------------|-------------|--------------|-------------|-------------|-------|-------------|-------------|---------------|-------------|-------|-------------|--------|-------------|--------------|-------|-------------|--------------|
| | | Params(M) | | | | | | | | | | | | | | | | | | | | |
| 64*2048 pixels | SqueezeSeg [51] | 29.5 | 1 | 85.4 | 54.3 | 26.9 | 4.5 | 57.4 | 68.8 | 3.3 | 16.0 | 4.1 | 3.6 | 60.0 | 24.3 | 53.7 | 12.9 | 13.1 | 0.9 | 29.0 | 17.5 | 24.5 |
| | SqueezeSegV2 [52] | 39.7 | 1 | 88.6 | 67.6 | 45.8 | 17.7 | 73.7 | 81.8 | 13.4 | 18.5 | 17.9 | 14.0 | 71.8 | 35.8 | 60.2 | 20.1 | 25.1 | 3.9 | 41.1 | 20.2 | 36.3 |
| | DarkNet21Seg [4] | 47.4 | 25 | 91.4 | 74.0 | 57.0 | 26.4 | 81.9 | 85.4 | 18.6 | 26.2 | 26.5 | 15.6 | 77.6 | 48.4 | 63.6 | 31.8 | 33.6 | 4.0 | 52.3 | 36.0 | 50.0 |
| | DarkNet53Seg [4] | 49.9 | 50 | 91.8 | 74.6 | 64.8 | 27.9 | 84.1 | 86.4 | 25.5 | 24.5 | 32.7 | 22.6 | 78.3 | 50.1 | 64.0 | 36.2 | 33.6 | 4.7 | 55.0 | 38.9 | 52.2 |
| 50K pts | RangeNet53++ [31] | 52.2 | 50 | 91.8 | 75.2 | 65.0 | 27.8 | 87.4 | 91.4 | 25.7 | 25.7 | 34.4 | 23.0 | 80.5 | 55.1 | 64.6 | 38.3 | 38.8 | 4.8 | 58.6 | 47.9 | 55.9 |
| | PointNet [34] | 14.6 | 3 | 61.6 | 35.7 | 15.8 | 1.4 | 41.4 | 46.3 | 0.1 | 1.3 | 0.3 | 0.8 | 31.0 | 4.6 | 17.6 | 0.2 | 0.2 | 0.0 | 12.9 | 2.4 | 3.7 |
| | SPG [23] | 17.4 | 0.25 | 45.0 | 28.5 | 0.6 | 0.6 | 64.3 | 49.3 | 0.1 | 0.2 | 0.2 | 0.8 | 48.9 | 27.2 | 24.6 | 0.3 | 2.7 | 0.1 | 20.8 | 15.9 | 0.8 |
| | SPLATNet [39] | 18.4 | 0.8 | 64.6 | 39.1 | 0.4 | 0.0 | 58.3 | 58.2 | 0.0 | 0.0 | 0.0 | 0.0 | 71.1 | 9.9 | 19.3 | 0.0 | 0.0 | 0.0 | 23.1 | 5.6 | 0.0 |
| 50K pts | PointNet++ [36] | 20.1 | 6 | 72.0 | 41.8 | 18.7 | 5.6 | 62.3 | 53.7 | 0.9 | 1.9 | 0.2 | 0.2 | 46.5 | 13.8 | 30.0 | 0.9 | 1.0 | 0.0 | 16.9 | 6.0 | 8.9 |
| | TangentConv [40] | 40.9 | 0.4 | 83.9 | 63.9 | 33.4 | 15.4 | 83.4 | 90.8 | 15.2 | 2.7 | 16.5 | 12.1 | 79.5 | 49.3 | 58.1 | 23.0 | 28.4 | 8.1 | 49.0 | 35.8 | 28.5 |
| | RandLA-NetV1 [16] | 50.3 | 0.95 | 90.4 | 67.9 | 56.9 | 15.5 | 81.1 | 94.0 | 42.7 | 19.8 | 21.4 | 38.7 | 78.3 | 60.3 | 59.0 | 47.5 | 48.8 | 4.6 | 49.7 | 44.2 | 38.1 |
| | RandLA-NetV3 [16] | 53.9 | 1.24 | 90.7 | 73.7 | 60.3 | 20.4 | 86.9 | 94.2 | 40.1 | 26.0 | 25.8 | 38.9 | 81.4 | 61.3 | 66.8 | 49.2 | 48.2 | 7.2 | 56.3 | 49.2 | 47.7 |
| PAI-Conv (ours) | 53.9 | 9.26 | 90.1 | 73.5 | 58.6 | 26.8 | 87.8 | 94.0 | 44.5 | 25.5 | 30.0 | 36.2 | 81.9 | 61.5 | 65.4 | 46.1 | 45.9 | 3.5 | 57.7 | 49.0 | 45.8 | |

Table 3: Quantitative results on Semantic3D [14].

| | mIoU(%) | OA(%) | man-made. | natural. | high veg. | low veg. | buildings | hard scape | scanning art. | car |
|------------------------|-------------|-------------|-------------|-------------|-------------|-------------|-------------|-------------|---------------|-------------|
| SnapNet [5] | 59.1 | 88.6 | 82.0 | 77.3 | 79.7 | 22.9 | 91.1 | 18.4 | 37.3 | 64.4 |
| SEGCloud [41] | 61.3 | 88.1 | 83.9 | 66.0 | 86.0 | 40.5 | 91.1 | 30.9 | 27.5 | 64.3 |
| RF_MSSF [42] | 62.7 | 90.3 | 87.6 | 80.3 | 81.8 | 36.4 | 92.2 | 24.1 | 42.6 | 56.6 |
| MSDeepVoxNet [37] | 65.3 | 88.4 | 83.0 | 67.2 | 83.8 | 36.7 | 92.4 | 31.3 | 50.0 | 78.2 |
| ShellNet [55] | 69.3 | 93.2 | 96.3 | 90.4 | 83.9 | 41.0 | 94.2 | 34.7 | 43.9 | 70.2 |
| GACNet [48] | 70.8 | 91.9 | 86.4 | 77.7 | 88.5 | 60.6 | 94.2 | 37.3 | 43.5 | 77.8 |
| SPG [23] | 73.2 | 94.0 | 97.4 | 92.6 | 87.9 | 44.0 | 83.2 | 31.0 | 63.5 | 76.2 |
| KPConv [43] | 74.6 | 92.9 | 90.9 | 82.2 | 84.2 | 47.9 | 94.9 | 40.0 | 77.3 | 79.7 |
| RandLA-NetV1 [16] | 76.0 | 94.4 | 96.5 | 92.0 | 85.1 | 50.3 | 95.0 | 41.1 | 68.2 | 79.4 |
| RandLA-NetV3 [16] | 77.4 | 94.8 | 95.6 | 91.4 | 86.6 | 51.5 | 95.7 | 51.5 | 69.8 | 76.8 |
| PAI-Conv (Ours) | 76.4 | 94.4 | 96.4 | 90.4 | 86.7 | 49.6 | 95.6 | 45.4 | 69.0 | 78.4 |

medium-sized single room around $20 \times 15 \times 5$ meters in 3D space. The S3DIS dataset includes 3D coordinates and RGB information that are used as the input for training and testing. The mIoU, mean class Accuracy (mAcc), and OA of the total 13 classes are used as the standard metrics.

Architecture. We adopt the network architecture from [16] and replace the LocSE module with our proposed PAI-Conv, where the size of kernel points is $L = 16$ and each point’s neighbors is $K = 16$. The network is an encoder-decoder architecture with skip connections. First, the input point cloud is fed to an MLP layer to extract per-point feature with output channel 8. Then, five encoder and five decoder networks are connected by an MLP layer. Each encoder layer consists of a residual block with a PAI-Conv layer and a random sampling operation. Through the five encoder layers, the point cloud is down-sampled with ratios of [4, 4, 4, 4, 2] and the feature dimension is increased with channels of [16, 64, 128, 256, 512]. In each decoder layer, the point feature is up-sampled by a nearest-neighbor interpolation and concatenated with the intermediate feature from the corresponding encoder layer through a skip connection. The concatenated feature is fed to an MLP layer. At last, three fully-connected layers with channels of [64, 32, num_class] and a dropout with 0.5 probability are used to finally predict the semantic label of each point.

Training. We use Adam optimizer with an initial learning rate of 0.01 and schedule the learning rate with decay 0.95 for 100 epochs. The training batch size is 6.

Results. Table 2, Table 3, and Table 4 present the quantitative results of different approaches on the SemanticKITTI, Semantic3D, and S3DIS dataset, respectively. PAI-Conv achieves on-par or better performance than state-of-the-art methods. Compared with the most recent RandLA-Net [16], PAI-Conv outperforms the version one (V1) of RandLA-Net in all the three datasets and is slightly lower than the version three (V3) of RandLA-Net in Semantic3D and S3DIS dataset. Note that, the small difference between RandLA-Net and PAI-Conv may be eliminated by repeatedly testing on the datasets. For SemanticKITTI dataset, two types of methods: point-based (**50K pts**) and projection-based (**64*2048 pixels**) are presented. DarkNet53Seg [4] and RangeNet53++ [31] achieve better results for some objects. However, they require costly steps for the pre/post projection.

Table 4: Quantitative results on the S3DIS dataset [1] (6-fold cross validation).

| | PointNet [34] | PointNet++ [36] | DGCNN [50] | 3P-RNN [54] | RSNet [18] | SPG [23] | LSANet [7] | PointCNN [26] | PointWeb [57] | ShellNet [55] | HEPIN [19] | KPCConv [43] | RandLA-Net V1 [16] | RandLA-Net V3 [16] | PAI-Conv (Ours) |
|---------|------------------|--------------------|---------------|----------------|---------------|-------------|---------------|------------------|------------------|------------------|---------------|-----------------|-----------------------|-----------------------|--------------------|
| OA(%) | 78.6 | 81.0 | 84.1 | 86.9 | - | 85.5 | 86.8 | 88.1 | 87.3 | 87.1 | 88.2 | - | 87.2 | 88.0 | 87.8 |
| mAcc(%) | 66.2 | 67.1 | - | - | 66.5 | 73.0 | - | 75.6 | 76.2 | - | - | 79.1 | 81.5 | 82.0 | 80.9 |
| mIoU(%) | 47.6 | 54.5 | 56.1 | 56.3 | 56.5 | 62.1 | 62.2 | 65.4 | 66.7 | 66.8 | 67.8 | 70.6 | 68.5 | 70.0 | 69.1 |

Table 5: The computation time, network parameters, and maximum number of input points of different approaches for semantic segmentation on Sequence 08 of the SemanticKITTI [4] dataset.

| | time (s) | para # (M) | point # (M) |
|------------------------|-------------|---------------|----------------|
| PointNet [34] | 192 | 0.8 | 0.49 |
| PointNet++ [36] | 9831 | 0.97 | 0.98 |
| PointCNN [26] | 8142 | 11 | 0.05 |
| SPG [23] | 43584 | 0.25 | - |
| KPCConv [43] | 717 | 14.9 | 0.54 |
| RandLA-Net [16] | 185 | 1.24 | 1.03 |
| PAI-Conv (Ours) | 176 | 9.26 | 1.51 |

Table 6: Ablation tests of classification results on the ModelNet40 for PAI-Cconv. We uniformly sample 1,024 points for each 3D shape.

| | MA(%) | OA(%) |
|---------------------|-------------|-------------|
| w/o permutation | 88.0 | 91.7 |
| w/o Sparsemax | 88.7 | 92.3 |
| w/ Softmax | 86.4 | 91.0 |
| w/ isotropic filter | 88.7 | 91.1 |
| w/ random kernel | 88.9 | 92.5 |
| w/ learnable kernel | 89.1 | 92.5 |
| full model | 90.0 | 92.9 |

4.3 Efficiency of PAI-Conv and ablation study

In this section, we conduct experiments to demonstrate the efficiency of PAI-Conv. Following the same setting of [16], we obtain the computation time, number of network parameters, and maximum number of input points of the proposed PAI-Conv for semantic segmentation on Sequence 08 of the SemanticKITTI [4] dataset on the machine with an AMD 3700X @3.6GHz CPU and an NVIDIA RTX2080Ti GPU. Maximum number of input points means the number of 3D points each network can take as input in a single pass to infer per-point semantics. As shown in Table 5, PAI-Conv achieves the shortest computation time and the largest number of input points. This is because, the same as RandLA-Net [16], we use random point sampling method instead of other expensive sampling methods. PAI-Conv is more efficient than RandLA-Net because we use fixed kernel points for dot production and only use one PAI-Conv layer instead of two for each residual block.

We conduct ablation tests on the ModelNet40 [53] to evaluate the effectiveness of the architecture design of PAI-Conv. We uniformly sample 1,024 points for each 3D shape. As shown in Table 6, When without permutation matrices (**w/o permutation**), the anisotropic filters are redundant since point clouds are irregular. When without Sparsemax (**w/o Sparsemax**) or replacing Sparsemax with Softmax (**w/ Softmax**), the permutation matrices are not sparse enough and become weighting matrices that tend to average each point’s neighbors. When replacing anisotropic filters with isotropic filters (**w/ isotropic filter**), all the points are treated equally, which is the same as PointNet [34]. When using random kernel points (**w/ random kernel**) or learnable kernel points (**w/ learnable kernel**), the local coordinates that define the canonical order cannot well cover each point’s local neighbors compared to the fixed kernel points generated using the Fibonacci lattice. Thanks to the design of PAI-Conv, the full model achieves the best results.

5 Conclusion

This paper proposes a permutable anisotropic convolutional operation (*PAI-Conv*) for point clouds. PAI-Conv is a physically meaningful generalization of CNN from grid-structured data to irregular data. Dot production attention and Sparsemax are used to obtain sparse soft-permeation matrices so that each point’s neighbors are rearranged in the canonical order of a set of fixed kernel points. Then anisotropic filters are applied to extract local features of point clouds. PAI-Conv can efficiently cooperate with random point sampling method and can be applied in large-scale point clouds. Quantitative experiments demonstrate that PAI-Conv produces competitive results with state-of-the-art methods on classification and semantic segmentation for point clouds.

References

- [1] Iro Armeni, Sasha Sax, Amir Roshan Zamir, and Silvio Savarese. Joint 2D-3D-semantic data for indoor scene understanding. *CoRR*, abs/1702.01105, 2017.
- [2] James Atwood and Don Towsley. Diffusion-convolutional neural networks. In *Proceedings of the 30th International Conference on Neural Information Processing Systems*, NIPS’16, page 2001–2009, Red Hook, NY, USA, 2016. Curran Associates Inc.
- [3] Matan Atzmon, Haggai Maron, and Yaron Lipman. Point convolutional neural networks by extension operators. *ACM Trans. Graph.*, 37(4), July 2018.
- [4] Jens Behley, Martin Garbade, Andres Milioto, Jan Quenzel, Sven Behnke, Cyrill Stachniss, and Jürgen Gall. SemanticKITTI: A dataset for semantic scene understanding of LiDAR sequences. In *The IEEE International Conference on Computer Vision (ICCV)*, October 2019.
- [5] Alexandre Boulch, Bertrand Le Saux, and Nicolas Audebert. Unstructured point cloud semantic labeling using deep segmentation networks. In *Proceedings of the Workshop on 3D Object Retrieval*, 3Dor ’17, page 17–24, Goslar, DEU, 2017. Eurographics Association.
- [6] André Brock, Theodore Lim, James M. Ritchie, and Nick Weston. Generative and discriminative voxel modeling with convolutional neural networks. *CoRR*, abs/1608.04236, 2016.
- [7] Lin-Zhuo Chen, Xuan-Yi Li, Deng-Ping Fan, Ming-Ming Cheng, Kai Wang, and Shao-Ping Lu. LSA-Net: Feature learning on point sets by local spatial aware layer. *arXiv preprint arXiv:1905.05442*, 2019.
- [8] Xiaozhi Chen, Huimin Ma, Ji Wan, Bo Li, and Tian Xia. Multi-view 3D object detection network for autonomous driving. In *The IEEE Conference on Computer Vision and Pattern Recognition (CVPR)*, July 2017.
- [9] Djork-Arné Clevert, Thomas Unterthiner, and Sepp Hochreiter. Fast and accurate deep network learning by exponential linear units (elus). *arXiv preprint arXiv:1511.07289*, 2015.
- [10] Theo Deprelle, Thibault Groueix, Matthew Fisher, Vladimir Kim, Bryan Russell, and Mathieu Aubry. Learning elementary structures for 3D shape generation and matching. In H. Wallach, H. Larochelle, A. Beygelzimer, F. d’Alché-Buc, E. Fox, and R. Garnett, editors, *Advances in Neural Information Processing Systems 32*, pages 7435–7445. Curran Associates, Inc., 2019.
- [11] Jacob Devlin, Ming-Wei Chang, Kenton Lee, and Kristina Toutanova. BERT: Pre-training of deep bidirectional transformers for language understanding. *arXiv preprint arXiv:1810.04805*, 2018.
- [12] Robert Dixon. Mathographics. basic blackwell limited, 1987.
- [13] Thibault Groueix, Matthew Fisher, Vladimir G. Kim, Bryan C. Russell, and Mathieu Aubry. 3D-CODED: 3D correspondences by deep deformation. In *The European Conference on Computer Vision (ECCV)*, September 2018.
- [14] Timo Hackel, N. Savinov, L. Ladicky, Jan D. Wegner, K. Schindler, and M. Pollefeys. SEMANTIC3D.NET: A new large-scale point cloud classification benchmark. In *ISPRS Annals of the Photogrammetry, Remote Sensing and Spatial Information Sciences*, volume IV-1-W1, pages 91–98, 2017.
- [15] Will Hamilton, Zhitao Ying, and Jure Leskovec. Inductive representation learning on large graphs. In I. Guyon, U. V. Luxburg, S. Bengio, H. Wallach, R. Fergus, S. Vishwanathan, and R. Garnett, editors, *Advances in Neural Information Processing Systems 30*, pages 1024–1034. Curran Associates, Inc., 2017.
- [16] Qingyong Hu, Bo Yang, Linhai Xie, Stefano Rosa, Yulan Guo, Zhihua Wang, Niki Trigoni, and Andrew Markham. RandLA-Net: Efficient semantic segmentation of large-scale point clouds. *Proceedings of the IEEE Conference on Computer Vision and Pattern Recognition*, 2020.
- [17] Binh-Son Hua, Minh-Khoi Tran, and Sai-Kit Yeung. Pointwise convolutional neural networks. In *The IEEE Conference on Computer Vision and Pattern Recognition (CVPR)*, June 2018.
- [18] Qiangui Huang, Weiyue Wang, and Ulrich Neumann. Recurrent slice networks for 3D segmentation of point clouds. In *The IEEE Conference on Computer Vision and Pattern Recognition (CVPR)*, June 2018.
- [19] Li Jiang, Hengshuang Zhao, Shu Liu, Xiaoyong Shen, Chi-Wing Fu, and Jiaya Jia. Hierarchical point-edge interaction network for point cloud semantic segmentation. In *The IEEE International Conference on Computer Vision (ICCV)*, October 2019.
- [20] Roman Klokov and Victor Lempitsky. Escape from cells: Deep kd-networks for the recognition of 3D point cloud models. In *The IEEE International Conference on Computer Vision (ICCV)*, Oct 2017.

- [21] Artem Komarichev, Zichun Zhong, and Jing Hua. A-CNN: Annularly convolutional neural networks on point clouds. In *The IEEE Conference on Computer Vision and Pattern Recognition (CVPR)*, June 2019.
- [22] Shiyi Lan, Ruichi Yu, Gang Yu, and Larry S. Davis. Modeling local geometric structure of 3D point clouds using Geo-CNN. In *The IEEE Conference on Computer Vision and Pattern Recognition (CVPR)*, June 2019.
- [23] Loic Landrieu and Martin Simonovsky. Large-scale point cloud semantic segmentation with superpoint graphs. In *The IEEE Conference on Computer Vision and Pattern Recognition (CVPR)*, June 2018.
- [24] Huan Lei, Naveed Akhtar, and Ajmal Mian. Octree guided CNN with spherical kernels for 3D point clouds. In *The IEEE Conference on Computer Vision and Pattern Recognition (CVPR)*, June 2019.
- [25] Jiaxin Li, Ben M. Chen, and Gim Hee Lee. SO-Net: Self-organizing network for point cloud analysis. In *The IEEE Conference on Computer Vision and Pattern Recognition (CVPR)*, June 2018.
- [26] Yangyan Li, Rui Bu, Mingchao Sun, Wei Wu, Xinhua Di, and Baoquan Chen. PointCNN: Convolution on \mathcal{X} -transformed points. In S. Bengio, H. Wallach, H. Larochelle, K. Grauman, N. Cesa-Bianchi, and R. Garnett, editors, *Advances in Neural Information Processing Systems 31*, pages 820–830. Curran Associates, Inc., 2018.
- [27] Ilya Loshchilov and Frank Hutter. SGDR: stochastic gradient descent with restarts. *CoRR*, abs/1608.03983, 2016.
- [28] Jiageng Mao, Xiaogang Wang, and Hongsheng Li. Interpolated convolutional networks for 3D point cloud understanding. In *The IEEE International Conference on Computer Vision (ICCV)*, October 2019.
- [29] Andre Martins and Ramon Astudillo. From softmax to sparsemax: A sparse model of attention and multi-label classification. In *International Conference on Machine Learning*, pages 1614–1623, 2016.
- [30] Daniel Maturana and Sebastian Scherer. VoxNet: A 3D convolutional neural network for real-time object recognition. In *2015 IEEE/RSJ International Conference on Intelligent Robots and Systems (IROS)*, pages 922–928, 2015.
- [31] Andres Milioto, Ignacio Vizzo, Jens Behley, and Cyrill Stachniss. RangeNet ++: Fast and accurate LiDAR semantic segmentation. In *2019 IEEE/RSJ International Conference on Intelligent Robots and Systems (IROS)*, pages 4213–4220, 2019.
- [32] Federico Monti, Davide Boscaini, Jonathan Masci, Emanuele Rodola, Jan Svoboda, and Michael M. Bronstein. Geometric deep learning on graphs and manifolds using mixture model CNNs. In *The IEEE Conference on Computer Vision and Pattern Recognition (CVPR)*, July 2017.
- [33] Charles R. Qi, Wei Liu, Chenxia Wu, Hao Su, and Leonidas J. Guibas. Frustum pointnets for 3D object detection from RGB-D data. In *The IEEE Conference on Computer Vision and Pattern Recognition (CVPR)*, June 2018.
- [34] Charles R. Qi, Hao Su, Kaichun Mo, and Leonidas J. Guibas. PointNet: Deep learning on point sets for 3D classification and segmentation. In *The IEEE Conference on Computer Vision and Pattern Recognition (CVPR)*, July 2017.
- [35] Charles R. Qi, Hao Su, Matthias Niessner, Angela Dai, Mengyuan Yan, and Leonidas J. Guibas. Volumetric and multi-view cnns for object classification on 3D data. In *The IEEE Conference on Computer Vision and Pattern Recognition (CVPR)*, June 2016.
- [36] Charles Ruizhongtai Qi, Li Yi, Hao Su, and Leonidas J. Guibas. PointNet++: Deep hierarchical feature learning on point sets in a metric space. In I. Guyon, U. V. Luxburg, S. Bengio, H. Wallach, R. Fergus, S. Vishwanathan, and R. Garnett, editors, *Advances in Neural Information Processing Systems 30*, pages 5099–5108. Curran Associates, Inc., 2017.
- [37] Xavier Roynard, Jean-Emmanuel Deschaud, and François Goulette. Classification of point cloud scenes with multiscale voxel deep network. *CoRR*, abs/1804.03583, 2018.
- [38] Martin Simonovsky and Nikos Komodakis. Dynamic edge-conditioned filters in convolutional neural networks on graphs. In *The IEEE Conference on Computer Vision and Pattern Recognition (CVPR)*, July 2017.
- [39] Hang Su, Varun Jampani, Deqing Sun, Subhransu Maji, Evangelos Kalogerakis, Ming-Hsuan Yang, and Jan Kautz. SPLATNet: Sparse lattice networks for point cloud processing. In *The IEEE Conference on Computer Vision and Pattern Recognition (CVPR)*, June 2018.

[40] Maxim Tatarchenko, Jaesik Park, Vladlen Koltun, and Qian-Yi Zhou. Tangent convolutions for dense prediction in 3D. In *The IEEE Conference on Computer Vision and Pattern Recognition (CVPR)*, June 2018.

[41] Lyne Tchapmi, Christopher Choy, Iro Armeni, Jun Young Gwak, and Silvio Savarese. SEGCloud: Semantic segmentation of 3D point clouds. In *2017 International Conference on 3D Vision (3DV)*, pages 537–547, 2017.

[42] Hugues Thomas, François Goulette, Jean-Emmanuel Deschaud, Beatriz Marcotegui, and Yann LeGall. Semantic classification of 3D point clouds with multiscale spherical neighborhoods. In *2018 International Conference on 3D Vision (3DV)*, pages 390–398, 2018.

[43] Hugues Thomas, Charles R. Qi, Jean-Emmanuel Deschaud, Beatriz Marcotegui, Francois Goulette, and Leonidas J. Guibas. KPConv: Flexible and deformable convolution for point clouds. In *The IEEE International Conference on Computer Vision (ICCV)*, October 2019.

[44] Ashish Vaswani, Noam Shazeer, Niki Parmar, Jakob Uszkoreit, Llion Jones, Aidan N Gomez, Łukasz Kaiser, and Illia Polosukhin. Attention is all you need. In I. Guyon, U. V. Luxburg, S. Bengio, H. Wallach, R. Fergus, S. Vishwanathan, and R. Garnett, editors, *Advances in Neural Information Processing Systems 30*, pages 5998–6008. Curran Associates, Inc., 2017.

[45] Petar Veličković, Guillem Cucurull, Arantxa Casanova, Adriana Romero, Pietro Liò, and Yoshua Bengio. Graph Attention Networks. *International Conference on Learning Representations*, 2018. accepted as poster.

[46] Nitika Verma, Edmond Boyer, and Jakob Verbeek. FeaStNet: Feature-steered graph convolutions for 3D shape analysis. In *The IEEE Conference on Computer Vision and Pattern Recognition (CVPR)*, June 2018.

[47] Chu Wang, Babak Samari, and Kaleem Siddiqi. Local spectral graph convolution for point set feature learning. In *The European Conference on Computer Vision (ECCV)*, September 2018.

[48] Lei Wang, Yuchun Huang, Yaolin Hou, Shenman Zhang, and Jie Shan. Graph attention convolution for point cloud semantic segmentation. In *The IEEE Conference on Computer Vision and Pattern Recognition (CVPR)*, June 2019.

[49] Shenlong Wang, Simon Suo, Wei-Chiu Ma, Andrei Pokrovsky, and Raquel Urtasun. Deep parametric continuous convolutional neural networks. In *The IEEE Conference on Computer Vision and Pattern Recognition (CVPR)*, June 2018.

[50] Yue Wang, Yongbin Sun, Ziwei Liu, Sanjay E. Sarma, Michael M. Bronstein, and Justin M. Solomon. Dynamic graph CNN for learning on point clouds. *ACM Trans. Graph.*, 38(5), Oct. 2019.

[51] Bichen Wu, Alvin Wan, Xiangyu Yue, and Kurt Keutzer. SqueezeSeg: Convolutional neural nets with recurrent CRF for real-time road-object segmentation from 3D LiDAR point cloud. In *2018 IEEE International Conference on Robotics and Automation (ICRA)*, pages 1887–1893, 2018.

[52] Bichen Wu, Xuanyu Zhou, Sicheng Zhao, Xiangyu Yue, and Kurt Keutzer. SqueezeSegV2: Improved model structure and unsupervised domain adaptation for road-object segmentation from a LiDAR point cloud. In *2019 International Conference on Robotics and Automation (ICRA)*, pages 4376–4382, 2019.

[53] Zhirong Wu, Shuran Song, Aditya Khosla, Fisher Yu, Linguang Zhang, Xiaou Tang, and Jianxiong Xiao. 3D ShapeNets: A deep representation for volumetric shapes. In *The IEEE Conference on Computer Vision and Pattern Recognition (CVPR)*, June 2015.

[54] Xiaoqing Ye, Jiamao Li, Hexiao Huang, Liang Du, and Xiaolin Zhang. 3D recurrent neural networks with context fusion for point cloud semantic segmentation. In *The European Conference on Computer Vision (ECCV)*, September 2018.

[55] Zhiyuan Zhang, Binh-Son Hua, and Sai-Kit Yeung. ShellNet: Efficient point cloud convolutional neural networks using concentric shells statistics. In *The IEEE International Conference on Computer Vision (ICCV)*, October 2019.

[56] Hengshuang Zhao, Li Jiang, Chi-Wing Fu, and Jiaya Jia. PointWeb: Enhancing local neighborhood features for point cloud processing. In *CVPR*, 2019.

[57] Hengshuang Zhao, Li Jiang, Chi-Wing Fu, and Jiaya Jia. PointWeb: Enhancing local neighborhood features for point cloud processing. In *The IEEE Conference on Computer Vision and Pattern Recognition (CVPR)*, June 2019.

[58] Yin Zhou and Oncel Tuzel. VoxelNet: End-to-end learning for point cloud based 3D object detection. In *The IEEE Conference on Computer Vision and Pattern Recognition (CVPR)*, June 2018.